DLR-IB-AS-BS-2022-63

Scale-resolving simulation of Vortex Separated Flows

V. Togiti, A. Krumbein, A. Probst
Institute of Aerodynamics and Flow Technology
$C^2A^2S^2E$

Deutsches Zentrum
DLR für Luft- und Raumfahrt

Bericht des Instituts für Aerodynamik und Strömungstechnik
Report of the Institute of Aerodynamics and Flow Technology

DLR-IB-AS-BS-2022-63

Scale-resolving Simulation of Vortex Separated Flows

V. Togiti, A. Krumbein, A. Probst

Herausgeber:
Deutsches Zentrum für Luft- und Raumfahrt e.V.
Institut für Aerodynamik und Strömungstechnik
Lilienthalplatz 7, 38108 Braunschweig

ISSN 1614-7790

Stufe der Zugänglichkeit: 1
Braunschweig, im Juli 2022

Institutsdirektor:
Prof. Dr.-Ing. habil. C.-C. Rossow

Verfasser:
V. Togiti, A. Krumbein, A. Probst

Abteilung: $C^2A^2S^2E$
Abteilungsleiter:
Prof. Dr. S. Görtz

Der Bericht enthält:
30 Seiten
15 Bilder
20 Literaturstellen

Contents

1. Introduction

Significant enhancements in computational fluid dynamics (CFD) have led to the use of numerical simulation in the design process of both civil and military aircraft, especially for nominal cruise performance where flows are generally characterized by attached flows. However, military vehicles routinely operate well outside of the steady, attached flow regimes often dominated by separated vortex flows. Therefore, major effort has to be devoted to ensure the vehicle qualified at many states that contain unsteady, highly separated flows. State-of-the-art CFD methods lack the ability to predict onset and progression of separated vortex-dominated flows, especially from smooth surfaces. Investigations carried out in several AVT task groups of the NATO Science and Technology Organization (STO) [1] indicate that the shortcomings for these predictions mainly stem from deficiencies of the models of turbulence. In most numerical investigations for slender wings with low sweep angle and blunt leading edges [2] linear eddy-viscosity turbulence models are employed. These models tend to deliver acceptable predictions at moderate incidence angles. However, at higher incidence angles, force coefficients and pitching moments were observed to be off compared to experiments. This is due to incorrect (earlier or delayed) prediction of incipient separation and differences in the strength of the subsequent development of vortices.

RANS turbulence models, eddy-viscosity models (EVM) and differential Reynolds stress models (RSM), are still the backbone of numerical simulations for industrial applications due to short turnaround time. Among RANS turbulence models, RSMs are considered suitable for vortex dominated flows due to the fact that in RSM individual transport equations are solved for the Reynolds stresses and the production term in the transport equations is treated exactly. Investigations conducted in [3] [4] also demonstrate the suitability of RSM for vortex dominated flows. However, vortex separated flows often are mildly or massively separated and highly unsteady. Numerical investigations of such flows involving complex flow phenomena often may not be well predicted by advanced RANS models, including RSM, and may require scale-resolving simulations (SRS) in which a small portion of turbulence is modeled and the rest is resolved. However, such methods require more computational resources compared to pure RANS simulations.

In this work, the objective is to assess the advantage of applying RSM over scale-resolving hybrid RANS/LES simulations for the flows involving separation from a smooth body and subsequent vortex formation. To this end, first, the predictions delivered by the RSM and the scale-resolving hybrid RANS/LES simulations based on eddy-viscosity-models are compared and their performance is assessed. Later, hybrid RANS/LES simulations based on the RSM are used and benefits of this method over the eddy-viscosity-based SRS are evaluated.

2. Details of Investigated Configurations

In the current study the flow over a delta wing and a diamond wing are investigated. These configurations unveil separation from a smooth surface and subsequent vortex formation. The flow over the delta wing is based on the experimental investigations carried out in the Vortex Flow Experiment-2 [5] at the DLR Göttingen. In the experiments, a 65° swept delta wing configuration with different rounded and sharp leading edges at angles of attack of 13.3 ° and 18 ° was investigated. In the experiments at the former incidence angle a partially developed separated vortex flow was observed while at the latter incidence angle a fully developed separated vortex flow was observed. In the current study the partially developed separated vortex flow case at a freestream Reynolds number based on the mean aerodynamic chord (c_{mac}) of $3x10^6$ and Mach number of 0.4 and the incidence angle of 13.3 ° with a medium radius rounded leading edge of $r/c_{mac} = 0.15\%$ is investigated. The flow topology at the aforementioned incidence angle is displayed in Figure *1* (a) which unveils vortex separation, inner and outer primary vortices.

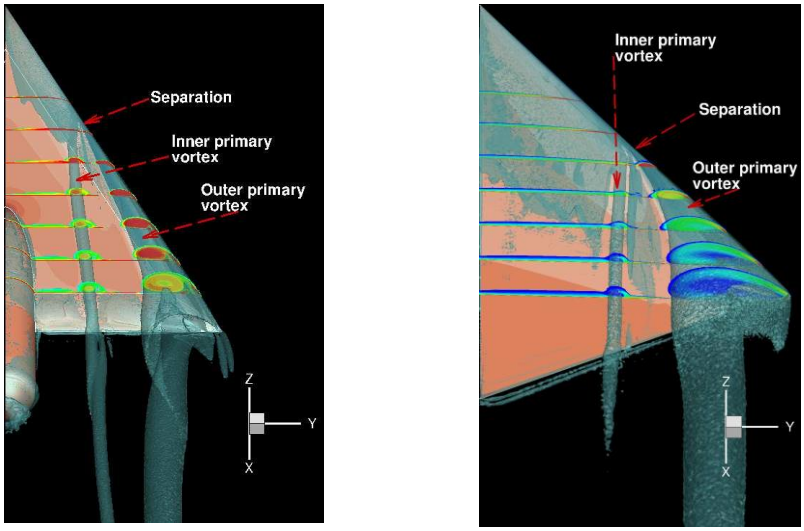

(a) Delta wing (b) Diamond wing

Figure 1: Flow topology on different configurations.

The other case investigated is the flow over a diamond wing which is based on the experimental study conducted in the NATO/AVT-183 task group [6] [7]. The geometry is a diamond wing with leading and trailing-edge sweeps of 53 ° and -26.5 °, respectively. In the experiments, the geometry is mounted on a tunnel floor wall with a peniche with standoff distance of $0.075c_r$, where c_r is the root chord which is 1.2m and tests were conducted at a free stream Mach number of 0.15 and Reynolds number based on the mean aerodynamic chord of $2.7x10^6$ and the incidence angle range of 10 ° to 15 ° with an increment of 1 °. For the present numerical investigation, the incidence angle of α = 12 ° was chosen as the flow separates midway along the blunt leading edge. Global flow

field characteristics associated to the incidence angle of 12 ^{o} are depicted in *Figure 1*(b) which displays flow separation and the inner and outer primary vortices.

3. Turbulence Modeling

Separated vortex flows investigated in the current study involve separation from a smooth body surface and formation of vortices. Often the vortex interaction with the attached boundary layer exposed to an adverse-pressure gradient leads to secondary vortices where anisotropy of normal Reynolds stresses is observed in experimental investigations [8]. Over the years, extensions to EVMs have been introduced to improve predictions of vortex flow and normal Reynolds stress anisotropy. In the present study, EVM coupled to a rotational correction (RC) approach [9] and the Quadratic Constitutive Relation (QCR) [10] which improve the prediction of the vortex strength and the anisotropy of normal Reynolds stresses are employed. As one of the objectives is to assess eddy-viscosity-based scale-resolving simulation (SRS) methods for flows involving separation from a smooth surface and subsequent vortex formation, the SA- and SA-RC-QCR-based delayed detached eddy simulation (DDES) [11] are considered. This approach combines RANS and LES in a way that in attached flow regions RANS is applied and in the separated regions large-eddy simulation (LES) is employed. The advantage of such a method is that flows involving massive separation and highly unsteady in nature are more accurately predicted compared to standard RANS approaches at a reasonable computational effort.

In the current investigation the test cases investigated demonstrate partially separated flow and this makes the accurate prediction of such flows with hybrid RANS-LES methods, here the DDES approach, challenging. In the discussion the results obtained by the DDES based on the SA and SA-RC-QCR are denoted SA-DDES and SA-RC-QCR-DDES, respectively.

Concerning RSMs, often the application of differential RSMs to flows involving complex flow phenomena leads to numerical stability problems due to numerical stiffness. This may be one of the reasons for not carrying out investigations with differential RSM in the earlier AVT studies [1]. Recently at DLR, a mathematically exact transformation of the length-scale-providing equation coupled to RSM was studied and demonstrated that such a transformation can significantly improve the stability of RSM for complex industrial flows. In the current study, the SSG/LRR Reynolds stress model [12] developed at DLR within the FLOMANIA project is considered. The ln(ω) length-scale equation [13] coupled to SSG/LRR-RSM, which improves the stability of RSM for complex flows, is employed in the current study and in the discussion the model predictions are denoted RSM.

Later, the DDES based on RSM is employed for the investigations. In this approach, analogously to the SST-DDES [14], the dissipation term in the Reynolds stress transport equation is modified for DDES. Here, the isotropic dissipation term is multiplied by the ratio of RANS and DDES length scales. In near-wall regions, the ratio of the length scale is one where the model acts as pure RANS. In separated regions, the length scale ratio is larger than one, where the DDES length scale is smaller than the RANS length scale. Due to this, the dissipation term increases and thereby reduces the modeled Reynolds stresses, which allows resolving turbulence. Details pertaining to RSM-based

DDES can be found in [15]. The results obtained by this variant of DDES is denoted by RSM-DDES in the discussion. In the present work, with the RSM-DDES, switching between RANS to LES is done using Menter's blending function F1 [16] in order to resolve vortices located very close to wall.

4. Numerical Methods

In the current investigation the unstructured compressible DLR flow solver TAU is used. Details about the DLR TAU code can be found in [17]. The inviscid fluxes of the main-flow equations are calculated by a central scheme with matrix artificial dissipation. For the turbulence equations, the convective fluxes are approximated with a second-order Roe scheme in the RSM and RSM-based DDES investigations and an Average-of-flux scheme in SA-RC-QCR and SA-RC-QCR-based DDES investigations. The viscous fluxes of the main flow and the diffusion fluxes of the turbulence equations are discretized using central differences.

For the DDES computations, low numerical dissipation is required in order to avoid excessive damping of resolved turbulent structures. In the current work, for the SA-DDES and SA-RC-QCR-DDES investigations the hybrid low-dissipation/low-dispersion (LD2) scheme is used, details can be found in [18]. However, for the RSM-DDES, such low dissipation leads to energy accumulation at high wave-numbers for the decaying isotropic turbulence case. In order to obtain the correct energy decay, the numerical dissipation is increased slightly, for details see [15].

.

5. Assessment of hybrid RANS/LES based on Eddy viscosity models

Here, the DDES based on SA and SA-RC-QCR are employed to assess the capabilities of standard hybrid RANS/LES methods for vortex separated flows. As the objective is to evaluate the potential advantages over RSM models for these flows, the DDES predictions are compared to RSM predictions and the experimental data. In this study the flow over delta wing and diamond wing at moderate incidence angle, mentioned in the previous sections, where partially separated flow prevail are investigated. It should be noted that the partially separated flows pose challenges to DDES as the flow separation stays very close to near wall regions where the hybrid model is neither fully in RANS mode, nor yet fully in LES mode. In this investigation, the advantages of applying DDES for the vortex separated flows is examined with respect to improvement of separation location and vortex strength.

In the DDES studies, the RANS results discussed earlier are used as an initial solution and advancement in time is carried out with a non-dimensional time step size of 0.001. Initially, the flow is let to develop over 4 to 5 convective time units and then time-averaging of the flow is carried out until time-averaged force coefficients settle down. In the current investigations, the time-averaging is carried out for about 10 CTUs. The grids used for the current investigation are the fine grids from the grid refinement study discussed in [19]. For the delta wing the grid has about 44 million grid nodes and the diamond wing grid has about 43 million nodes.

5.1. Delta wing

To unveil the instantaneous flow topology delivered by RSM, SA-DDES and SA-RC-QCR-DDES the iso-surface of $\lambda 2$ and the vorticity magnitude contours at different streamwise sections are depicted in Figure 2. With the RSM, flow separation occurs at x/cr = 0.4 and forms the outer primary vortex. According to [1], a part of the flow from the outer primary vortex moves towards the inboard section of the wing after reattachment and its interaction with the attached flow from the apex leads to the inner primary vortex which is delivered with the RSM. In the case of SA-DDES flow separation occurs at about x/cr = 0.48 and forms the inner primary and outer primary vortices. However, in contrast to the RSM results and the experiments, the inner primary vortex merges with the outer primary vortex a short distance downstream of the vortex separation. With the SA-RC-QCR-DDES flow separation is predicted at x/cr = 0.3 which is upstream of the separation observed with the SA-DDES and RSM, see Figure 2(c). Concerning the inner and outer primary vortices, the SA-RC-QCR-DDES predicts both vortices. In both DDES investigations parallel vortices aligned with the flow direction are resolved on the inboard section of the wing. In the experimental investigations the existence of parallel aligned vortices on the inboard section of the wing has not been discussed.

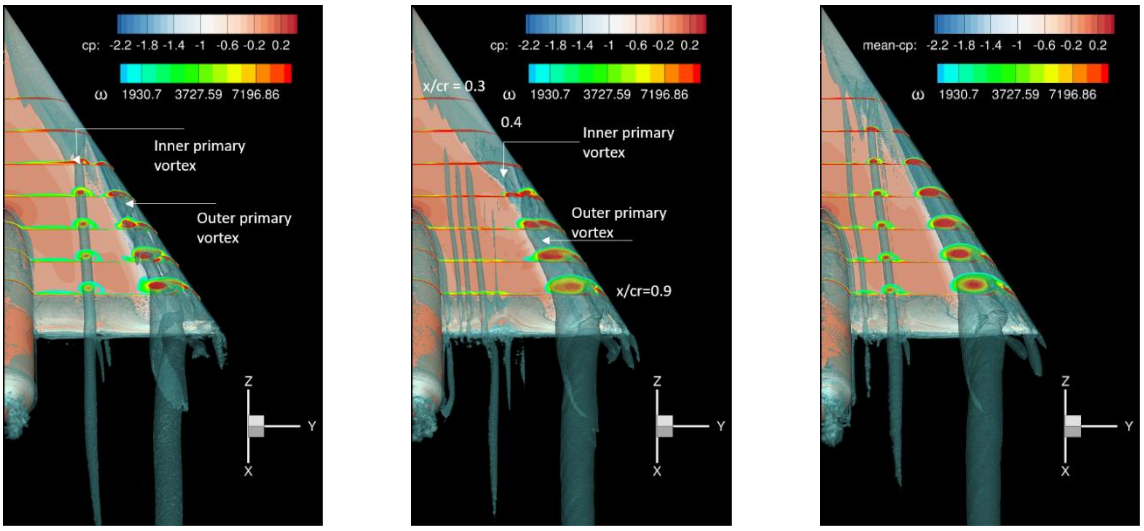

(a) RSM (b) SA-DDES (c) SA-RC-QCR-DDES

Figure 2: Contours of vorticity magnitude and the iso surface of λ_2 of the time-averaged flow field on the delta wing.

Figure 3 presents the surface pressure distribution on the suction side of the wing from the experiments and the predictions delivered by the RSM and DDES computations. In the experiments the movement of the suction pressure from the leading edge to the inboard section of the wing indicates flow separation and subsequent formation of an outer primary vortex, see Figure 3(a). From the contours of the experiments, it is apparent that the separation occurs at $x/c_r = 0.48$. In the figure the suction pressure associated with the outer primary vortex is depicted with a blue streak. A bit inboard from the outer primary vortex another local cpmin streak in the experiment illustrates an inner primary vortex.

In the RSM predictions the flow separates from the leading edge at about $x/c_r = 0.4$, and inner and outer primary vortices can be observed. The inner primary vortex is located slightly inboard in the RSM results compared to the experiments as the separation is predicted earlier than in the experiments. Concerning the pressure associated with the outer primary vortex, the cp level delivered in the RSM predictions agrees with the experiments, however, its position is located slightly inboard.

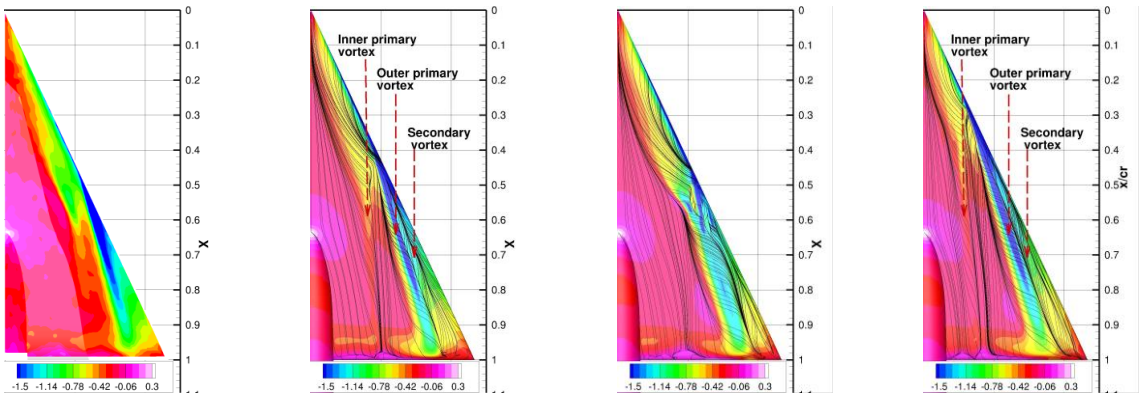

(a) Exp. (b) RSM (c) SA-DDES (d) SA-RC-QCR-DDES

Figure 3: Contours of pressure coefficient and skin-friction lines on delta wing.

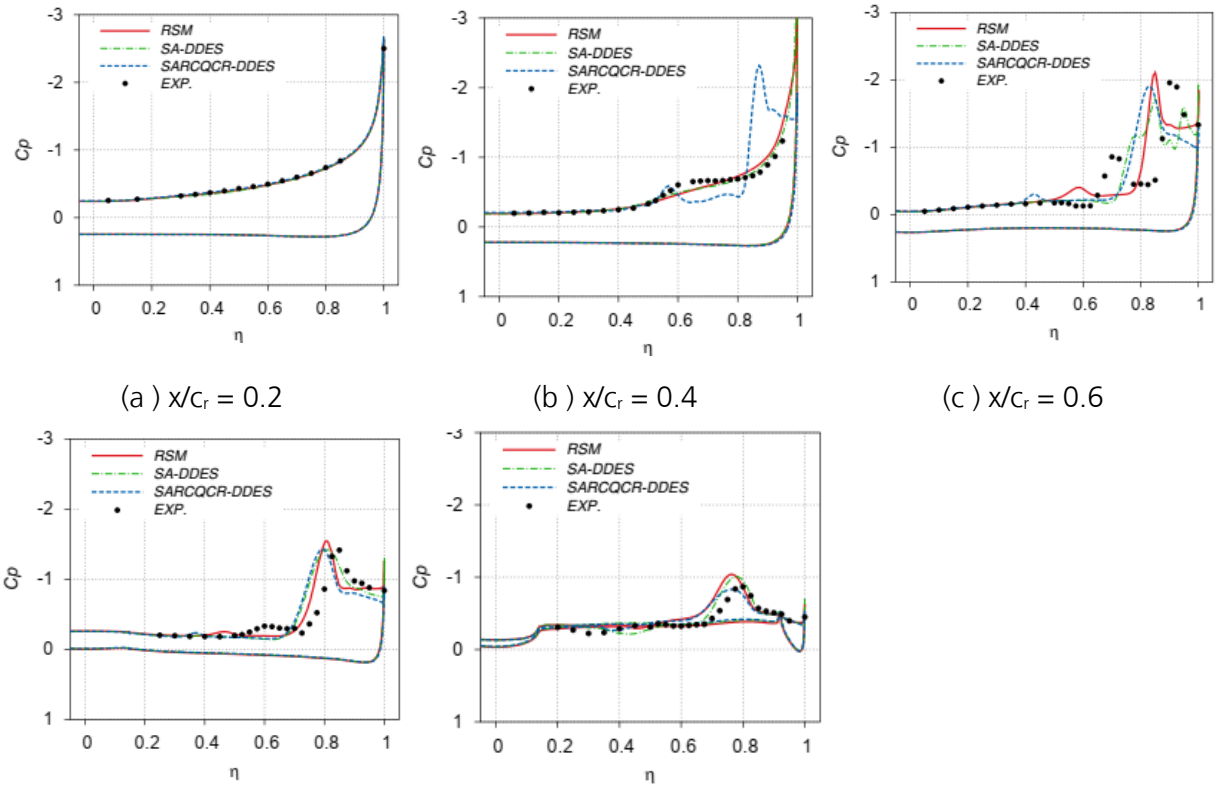

(a) $x/c_r = 0.2$ (b) $x/c_r = 0.4$ (c) $x/c_r = 0.6$

(d) $x/c_r = 0.8$ (e) $x/c_r = 0.95$

Figure 4: Sectional cp distribution on delta wing.

In the SA-DDES predictions, the flow separates at about $x/c_r = 0.48$ and forms the outer primary vortex, see Figure 3(c). The pressure associated with the vortex is higher than in the experiments. Furthermore, the inner primary vortex is not predicted. In the SA-RC-QCR-DDES

predictions the flow separates from the leading edge at about $x/c_r = 0.3$ and forms both the inner and outer primary vortices, see Figure 3(d). The location of flow separation is predicted too far upstream compared to the experiments and the RSM predictions. This upstream movement of separation resulted in a more inboard located inner primary vortex. In spite of the more inboard located vortices, the suction pressure associated with the outer vortex is closer to the experiments. The comparison of the sectional pressure distribution is shown in Figure *4*. At the streamwise station of $x/c_r = 0.2$, attached flow pressure distribution is observed in the experiments. This trend is reproduced in all the predictions. At $x/c_r = 0.4$, see Figure 4(b), the suction peak is located at the leading edge which unveils attached flow in the experiments. In addition to this the experimental cp shows a plateau on the inboard section which indicates the flow on the verge of separation. In the RSM and SA-DDES predictions attached flow trend is delivered. Both models failed to deliver cp plateau on the inboard section of wing. In SA-RC-QCR-DDES the suction peak is located inboard which indicates earlier vortex separation. And the two suction peaks at $\eta = 0.86$ and 0.58 unveil the locations of the outer primary vortex and the inner primary vortex, respectively. At this location the predictions of SA-RC-QCR-DDES do not show the experimental trends

At $x/c_r = 0.6$, the experiments show a vortex separation trend and unveil two suction peaks which render the pressure associated with the inner and outer primary vortices and their locations. In the experiments the outer primary vortex is located at η of about 0.9 and the inner primary vortex is located at η of about 0.7. As can be seen in the Figure 4(c), all the models predict the outer primary vortex more inboard compared to the experiments. In the RSM-ln(ω) and SA-RC-QCR-DDES predictions the suction peak level associated with the outer primary vortex agrees with the experiments. In the SA-DDES predictions the lower suction peak of the outer primary vortex is because of the weaker vortex compared to the other predictions and experiments.

The suction pressure of the inner primary vortex is underpredicted in the RSM and SA-RC-QCR-DDES results which indicate that the strength of the inner primary vortex in the predictions is considerably weaker than in the experiments. Concerning the location of the inner primary vortex, both modeling approaches deliver the inner primary vortex more inboard compared to the experiments. The reason for the more inboard located inner primary vortex is the more upstream prediction of flow separation compared to the experiments. In the SA-DDES predictions the suction pressure associated with the inner primary vortex is not observed as it fails to capture the vortex on this grid. Farther downstream at $x/c_r = 0.8$ and 0.95, more inboard located inner and outer primary vortices compared to experiments are delivered by RSM and a weaker inner primary vortex compared to experiments is computed by SA-RC-QCR-DDES.

5.1.1. Discussion on the capabilities of EVM based SRS for the delta wing

For the delta wing considered in the present study, the experimental data unveil flow separation midway along the leading edge and the presence of outer and inner primary vortices. The SA-DDES delivers the experimental vortex separation location and predicts the inner primary and outer primary vortices. However, in contrast to the experiments, a short distance after the inception of the inner primary vortex, fusion of the inner primary and outer primary vortices is observed. Additionally, the strength of the outer primary vortex is predicted too weak compared to experiments.

When the SA-DDES is coupled with the rotational correction and quadratic constitutive relation, it predicted separation too far upstream of experimental separation location. This leads to more inboard located inner and outer primary vortices. These additional extensions have not improved the prediction of the strength of vortices. A possible reason for the upstream movement of separation location is the rotation/curvature correction term which is usually active on the leading-edge region that reduces turbulence level in the boundary layer that may have led to earlier separation.

For partially separated flows, such as these, the accurate prediction of vortex separation is decisive for the downstream development of the vortex. In the RANS performance study, it is observed that the use of the rotational correction and quadratic constitutive relation extensions with the SA lead to more upstream movement of separation location compared to the experiments. In the present study, the same trend is observed in the SA-RC-QCR-DDES investigations as the SA-RC-QCR turbulence model is employed in the near wall region. From this study, it seems the use of additional extensions may not be necessary for the prediction of these partially separated flows.

On the given grids and based on the solver settings applied for this configuration, the RSM shows the tendency to represent the flow slightly better than the DDES by delivering separation locations closer to experiments and stronger outer and inner primary vortices compared to the other methods employed.

5.2. Diamond wing

Figure 5 shows the iso-surface of $\lambda 2$ along with vorticity contours of the time-averaged flow field. As can be seen in the RSM predictions the flow separation and subsequent vortex formation occurs about $x/c_r = 0.3$ while in SA-DDES it occurs at about $x/c_r = 0.35$ which agrees with the experimental finding. In the case of SA-RC-QCR-DDES the vortex separation occurs at $x/c_r = 0.25$ which is far too upstream of the trend observed in the SA-DDES. On the inboard section of the wing, an additional weak inner primary vortex is predicted in the RSM predictions. A similar trend is also delivered in both variants of DDES investigations.

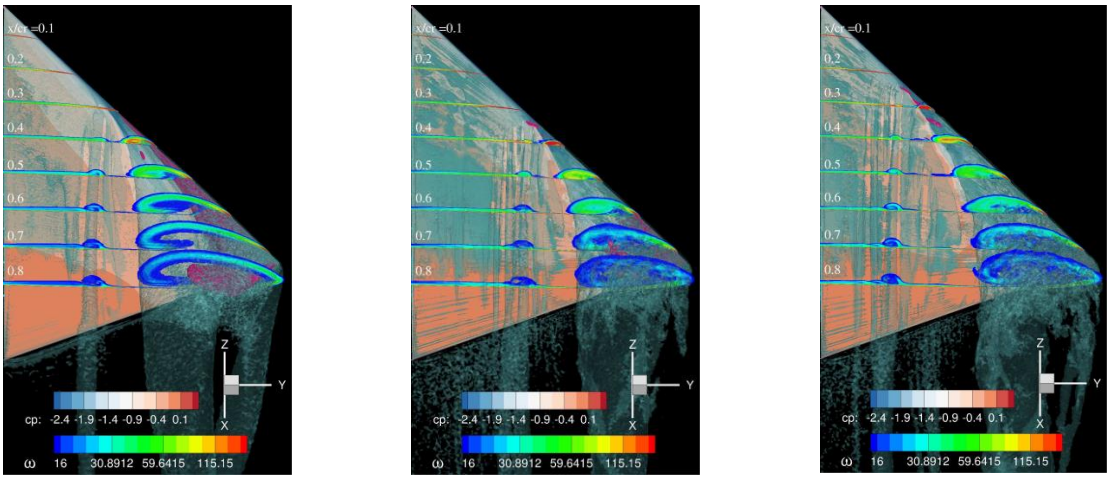

(a) RSM (b) SA-DDES (c) SA-RC-QCR-DDES

Figure 5: Contours of the vorticity magnitude and iso-surface of λ_2 of the time-averaged flow field for the diamond wing.

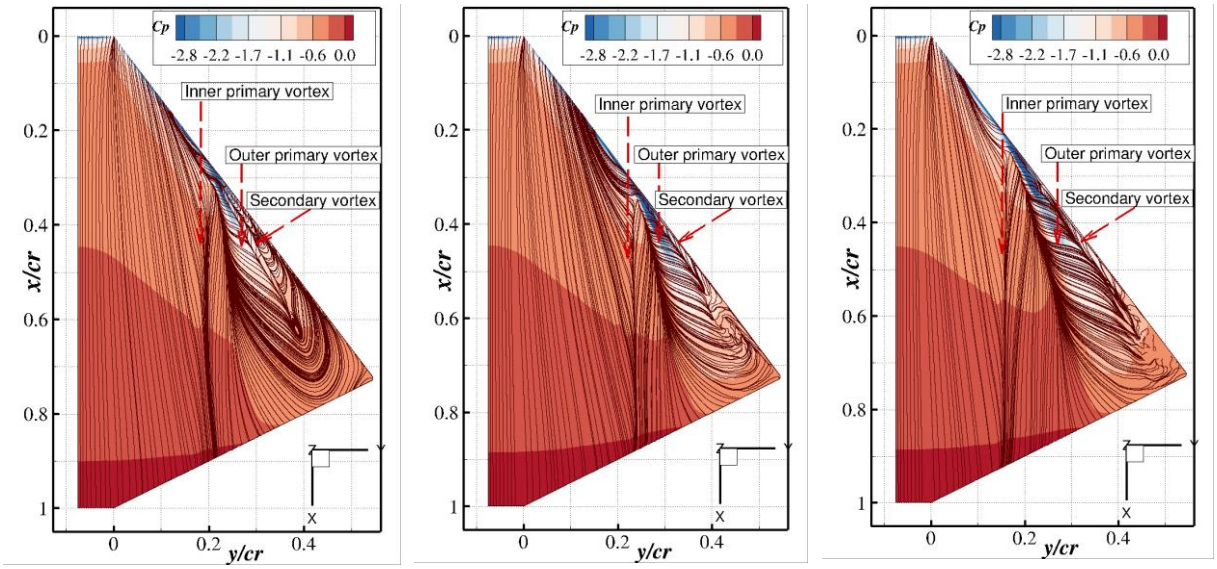

(a) RSM (b) SA-DDES (c) SA-RC-QCR-DDES

Figure 6: Contours of pressure coefficient and skin-friction lines.

In Figure 6 the surface pressure distribution along with the skin-friction lines are shown. As is visible from the figures, the foot prints unveil the predicted inner primary and outer primary vortices yielded by all the models. In the case of SA-RC-QCR-DDES the inner primary vortex is located more inboard compared to the other two predictions. In the RSM predictions the location of the inner primary vortex is a bit outboard compared to the SA-RC-QCR-DDES and inboard compared to the

SA-DDES. Apparently, the position of the inner primary vortex depends on the vortex separation location. The earlier the vortex separation the more inboard located is the inner primary vortex.

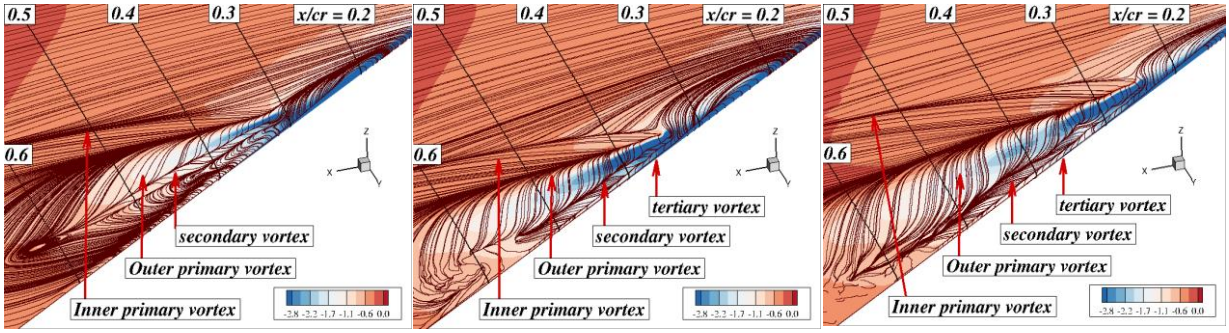

(a) RSM (b) SA-DDES (c) SA-RC-QCR-DDES

Figure 7:Close-up view of leading edge with the contours of pressure coefficient and skin-friction lines.

To visualize further the predicted vortices, a close-up view of the leading-edge region is shown in Figure 7. In the SA-DDES and SA-RC-QCR-DDES cases secondary and tertiary vortices are predicted. In the case of RSM, in addition to these vortices, a whirl can be observed where the outer primary vortex collapses with the secondary vortex.

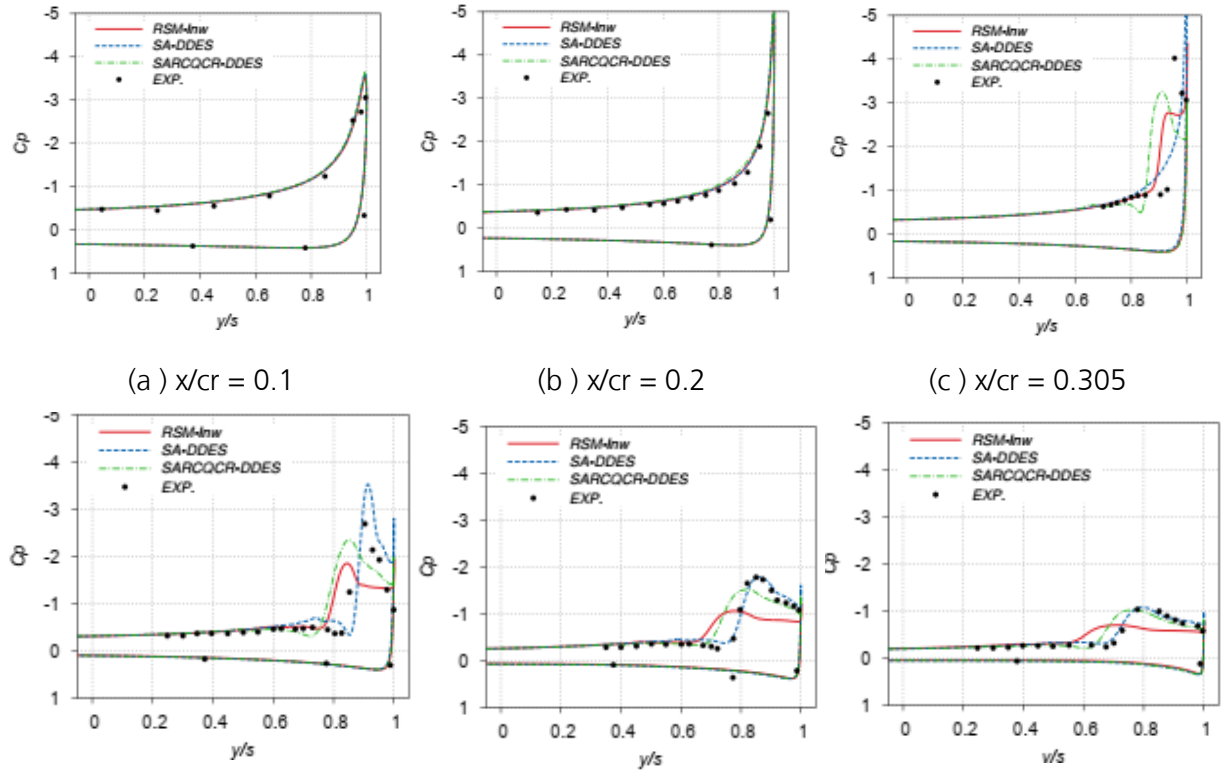

(a) x/cr = 0.1 (b) x/cr = 0.2 (c) x/cr = 0.305

(d) x/cr = 0.405 (e) x/cr = 0.5 (f) x/cr = 0.6

Figure 8: Cp distribution at different streamwise sections.

The comparison of the sectional pressure distribution is displayed in Figure 8. At the streamwise sections of x/cr = 0.1 and x/cr = 0.2 the experiments show the trend of an attached flow. This trend is reproduced in the predictions with all the turbulence models applied. At x/cr = 0.305, in the experiments the inboard movement of the suction peak from the leading edge indicates flow separation and subsequent vortex formation. The location of the suction peak also indicates the vortex axis. As can be seen in Figure 8**,** the SA-DDES predicts attached flow at this location while SA-RC-QCR-DDES delivers the experimental trend, however, the predicted vortex axis is more inboard compared to the experiments which is because of the earlier vortex separation than in the experiments. In the RSM prediction, the flow is still attached with the suction peak at the leading edge. A plateau in cp on the inboard leading edge indicates the flow is on the verge of separation in the RSM.

At x/cr = 0.405, in the experiments a lower suction peak compared to the previous location is observed. This is because with the downstream distance the size of the vortex grows and its strength decreases. The location of cp_{min} indicates that the vortex core axis moves inboard with the downstream distance. At this streamwise station the predictions of the SA-DDES are in good agreement with experimental data with regard to the vortex position and the cp level associated with it. The SA-RC-QCR-DDES predicts the vortex more inboard and delivers lower cp compared to the experiments as a weaker vortex is predicted. In RSM the position of the vortex is predicted more inboard and delivers lower cp compared to the experiments. From the contours of the vorticity magnitude, see **Error! Reference source not found.**, and the cp level it is apparent that the p redicted vortex in RSM is the weakest. At farther downstream locations the vortex core axis and the cp levels are well predicted by the SA-DDES. Both the SA-RC-QCR-DDES and RSM deliver the vortex more inboard and lower cp compared to the experiments.

Though the SA-DDES predicts the vortex separation slightly downstream of the experimental location, it delivers the cp associated with the vortex and its position much better than the other turbulence model predictions. Overall, for this test case the SA-DDES performs better than the other modeling approaches applied.

6. Assessment of hybrid RANS/LES based on a Reynolds-stress model

In this section investigations carried out with the DDES based on RSM are discussed. To assess the performance of the RSM-DDES, the predictions obtained for different configurations are compared to the experimental data and predictions of RSM and SARCQR-DDES.

6.1. Delta wing

The global feature of the flow is unveiled in Figure 9 by showing the iso-surface of λ2 along with the contours of vorticity magnitude of the time-averaged flow field. In the figure, streamwise sections are located from x/c_r = 0.3 to 0.9 with a distance between each station of 0.1. In all the predictions, both the outer primary and inner primary vortices are delivered. In RSM-DDES and SA-RC-QCR-DDES predictions, flow separation from leading edge and formation of outer primary and inner primary vortices occur upstream of x/c_r = 0.3, which is earlier than in the RSM predictions. In cases of RSM-DDES and SA-RC-QCR-DDES, one more streamwise vortex aligned with the freestream is resolved. As it can be seen in the figure the streamwise extent of this vortex is longer in SA-RC-QCR-DDES compared to RSM-DDES.

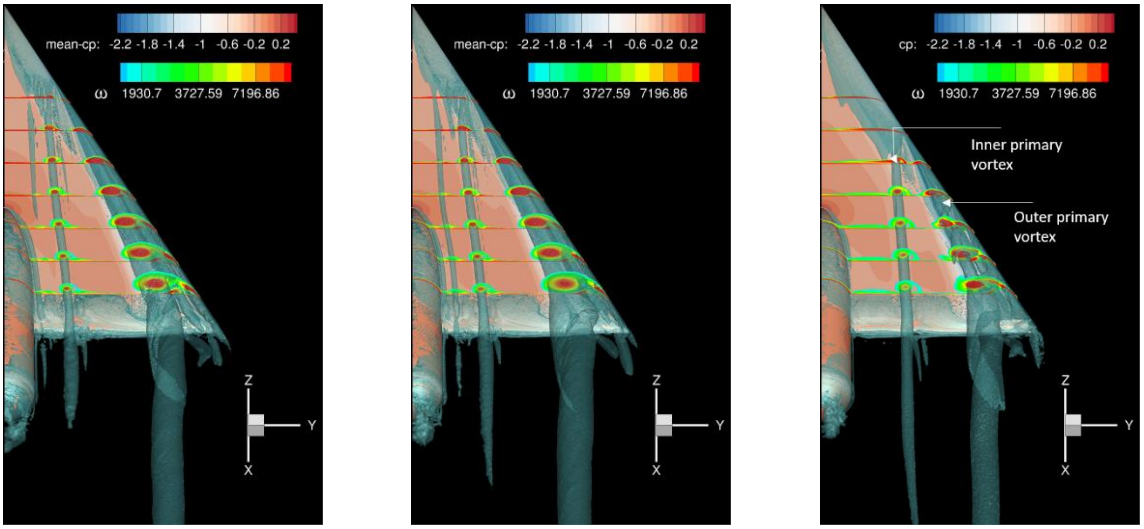

(a) RSM-DDES (b) SA-RC-QCR-DDES (c) RSM

Figure 9: Contours of vorticity magnitude and the iso surface of λ_2 on delta wing of the time-averaged flow field.

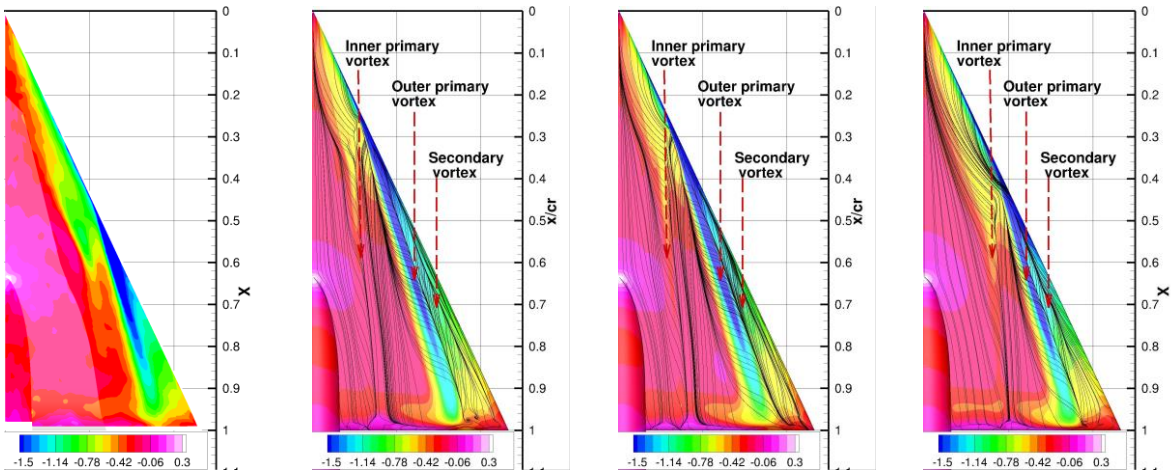

(a) Exp. (b) RSM-DDES (c) SA-RC-QCR-DDES (d) RSM

Figure 10: Contours of pressure coefficient and skin-friction lines of time-averaged field on delta wing.

Contours of surface pressure distribution delivered by different models is shown in Figure 10 and compared with the experimental data. Additionally, the surface skin-friction lines in the numerical investigations are shown to render the vortex footprint. In the experiments, the movement of suction pressure from the leading edge towards the inboard section indicates the flow separation and formation of the outer primary vortex. In the experiments, based on the cp distribution, flow separation appears to occur at the streamwise station of $x/c_r = 0.48$. In the predictions, this trend is observed more upstream than in the experiments.

A bit inboard from the separation point in the experiments, a local cp minimum in the region, shown with green color, render the origin of the inner primary vortex and associated pressure with it. In the predictions, the location is observed to be more inboard and the pressure associated with the vortex is higher compared to the experiments. The reason for the more inboard located inner primary vortex is the more upstream flow separation in predictions.
In all the DDES investigations, earlier flow separation is predicted compared to the experiments. Among all the predictions, the separation location delivered by the RSM is in closer agreement with the experiments.

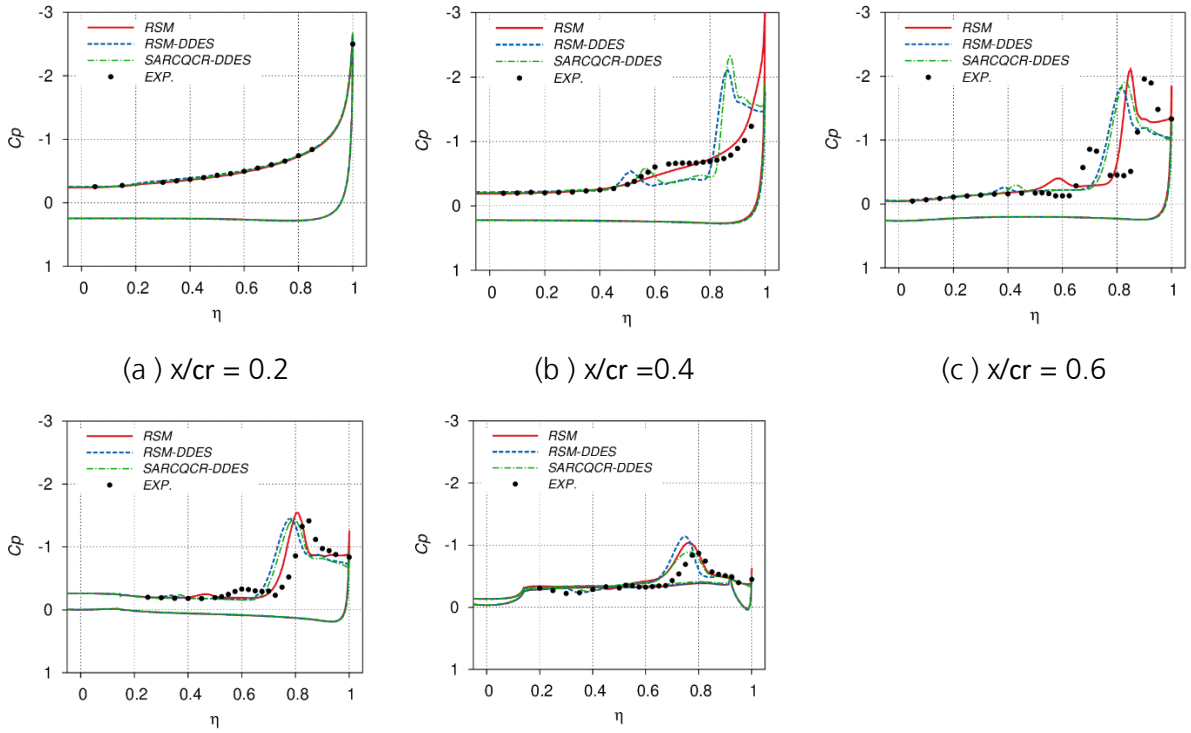

(a) x/cr = 0.2 (b) x/cr =0.4 (c) x/cr = 0.6

(d) x/cr = 0.8 (e) x/cr = 0.95

Figure 11: Sectional cp distribution on delta wing.

In Figure 11, the sectional pressure distribution from the simulations is compared to the experimental data. At the streamwise section x/c_r = 0.2, attached flow is observed in the experiments. A similar trend is delivered in all the predictions. Downstream of the aforementioned location at x/c_r = 0.4, the experimental pressure distribution still shows attached flow trend. A plateau in cp distribution indicates the flow on the verge of separation. In contrast to the experiments, in both scale-resolving predictions, loss of suction peak at the leading edge is delivered due to flow separation and subsequently local suction peaks at spanwise location η of 0.85 and 0.6 caused by the formation of outer primary vortex and inner primary vortex, respectively. With RSM, similar to the experiments, attached flow is observed at this streamwise location.

At x/c_r = 0.6, the experimental pressure distribution shows the presence of outer and inner-primary vortices with the suction peaks at spanwise location η of 0.9 and 0.7, respectively. At this location, all the predictions reproduce the experimental trend. However, the locations of both vortices are delivered more inboard due to earlier flow separation compared to the experiments. Concerning the vortex strength, shown with the level of suction peak, all DDES simulations delivered weaker outer primary vortex and this resulted in lower suction peak associated with the vortex. For the inner primary vortex, much weaker vortex compared to the experiments is predicted in all the predictions. In RSM predictions, since the vortex flow separation is closer to the experiments, the

suction peak associated with the outer primary vortex agrees well with the experiments. However, the suction peak of the inner primary vortex is underpredicted.
At further downstream locations, lower suction peaks for the inner and outer primary vortices compared to the upstream sections are observed in the experiments. This trend is reproduced in all the predictions. However, the vortices are located more inboard compared to the experiments.
The applied SA-RC-QCR-DDES and RSM-DDES approaches on the grids employed in this study do not show any improvement in the predictions compared to the unsteady RSM for this configuration. The DDES with SA-RC-QCR and RSM deliver earlier flow separation from the round leading edge which leads to earlier formation of outer and inner primary vortices compared to the experiments, while the unsteady RSM predicted flow separation closer to the experimental separation location. The upstream movement of the separation location in SA-RC-QCR-DDES is attributed to the underlying RANS turbulence model, SA-RC-QCR. In RSM-DDES, earlier flow separation is caused by the modelled-stress-depletion [11], more details in the discussion section.

6.2. Diamond wing

An iso surface of λ_2 and slices with the vorticity magnitude of the time average flow field are shown in Figure 12. As it can be seen in the figure, flow separation from the leading edge and subsequent formation of outer primary vortex occurs at about x/cr = 0.2 in RSM-DDES. In the case of SA-RC-QCR-DDES, flow separation occurs at x/cr = 0.25. In contract, in RSM flow separation is predicted at x/cr = 0.3, which is the most downstream location compared to the other predictions. In the experiments, vortex separation at is observed upstream of x/cr = 0.3. In all the predictions, the outer primary vortex and a weak inner primary vortex is predicted, which agrees with the experimental trend. In the predictions of RSM-DDES and SA-RC-QCR-DDES, additional streamwise vortices parallel to inner primary vortex are resolved. A trend that is also observed of the delta wing with scale-resolving methods.

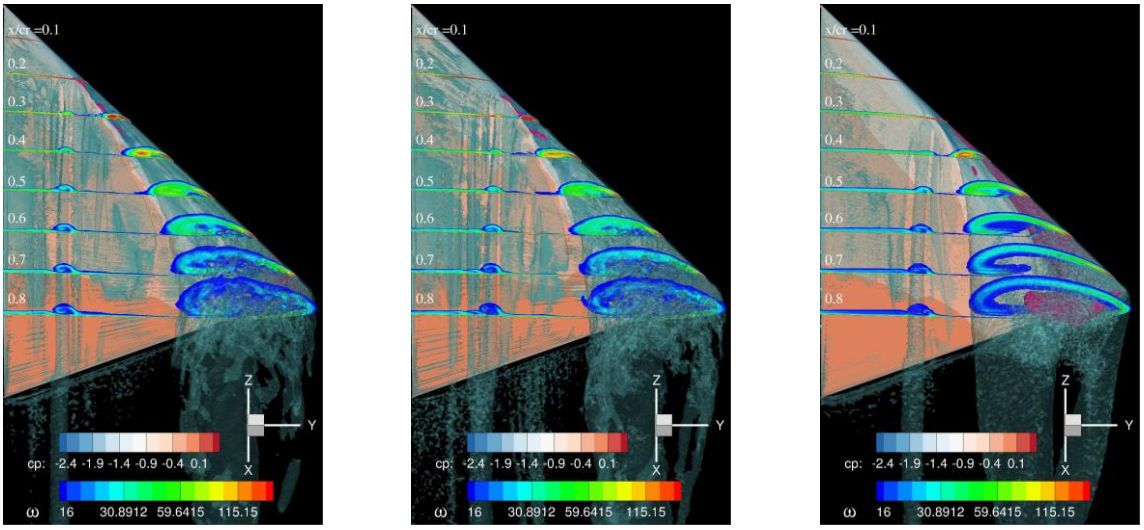

(a) RSM-DDES (b) SA-RC-QCR-DDES (c) RSM

Figure 12: Contours of the vorticity magnitude and iso-surface of λ_2 of the time-averaged flow field for the diamond wing.

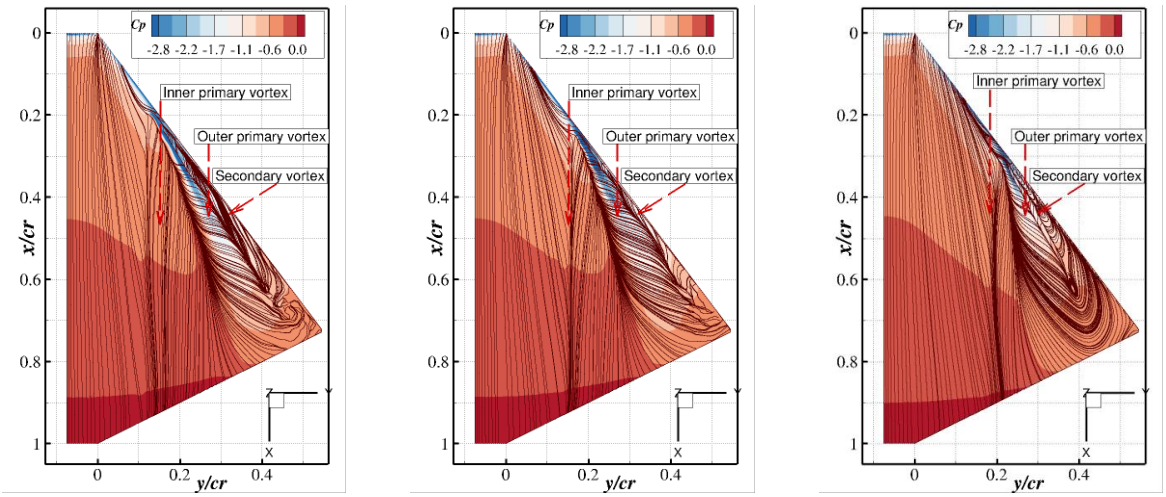

(a) RSM-DDES (b) SA-RC-QCR-DDES (c) RSM

Figure 13: Surface skin-friction lines and the contours of pressure coefficient.

The skin-friction lines along with the surface pressure distribution on the suction side of the wing are displayed in Figure 13. The skin-friction lines unveil the predicted inner primary and outer primary vortices by all the applied models. Additionally, there is also the evidence of a secondary vortex in all the predictions near the leading edge of the wing. In the DDES investigations based on RSM, a larger spanwise extend secondary vortex is predicted compared to SA-RC-QCR-based DDES. From the counters of cp on the surface, it is evident that the suction pressure associated with the

outer primary vortex in RSM-DDES is almost the same as in SA-RC-QCR-DDES, indicating almost same vortex strength in the predictions.

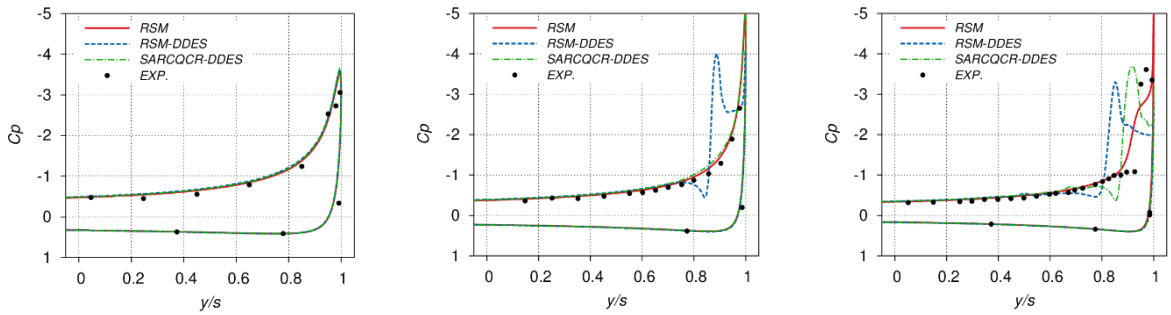

(a) x/cr = 0.1 (b) x/cr = 0.2 (c) x/cr = 0.295

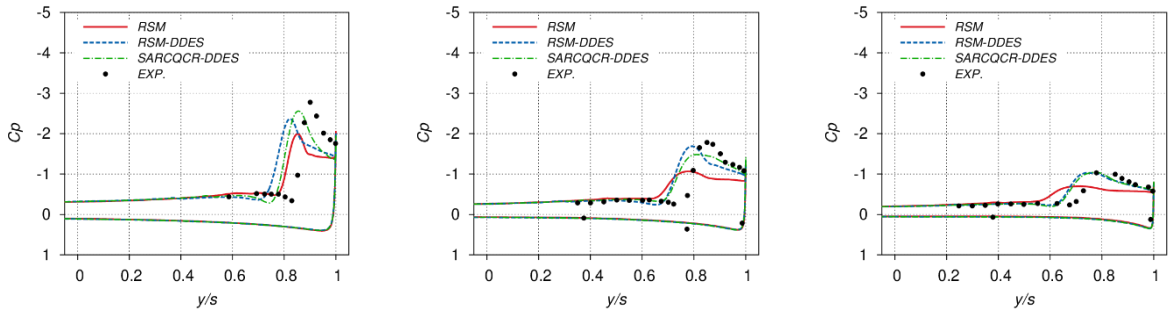

(d) x/cr = 0.395 (e) x/cr = 0.5 (f) x/cr = 0.6

Figure 14: Cp distribution at different streamwise sections.

The comparison of the sectional pressure distribution is displayed in Figure 14. Here the RSM results are shown for reference. At the streamwise sections of $x/c_r = 0.1$ the RSM-DDES predicts attached flow. However, at $x/c_r = 0.2$, it predicts vortex separation as a result of the suction peak at the leading-edge collapses. At $x/c_r = 0.295$, in the experiments the inboard movement of the suction peak from the leading edge indicates flow separation and subsequent vortex formation. The location of the suction peak also indicates the vortex axis.

As can be seen in Figure 14 (c), all DDES predictions follows the experimental trend, however, the predicted vortex axis is more inboard compared to the experiments which is because of the earlier vortex separation than in the experiments.

In RSM-DDES, the vortex axis is located most inboard while in SA-RC-QCR the location is closer to the experiments. The reason for this trend is the flow separation which is predicted too far upstream in RSM-DDES while the SA-RC-QCR-DDES predicts the separation location closer to experimental data.

At $x/c_r = 0.395$, in the experiments a lower suction peak compared to the previous location is observed. This is because with the downstream distance the size of the vortex grows and its strength decreases. The location of cp_{min} indicates that the vortex core axis moves inboard with the

downstream distance. At this streamwise station all the DDES predictions deliver the same cp level. At farther downstream locations almost the same level of cp peaks and the vortex core axis are predicted by all the DDES models.

Overall for this configuration, the DDES based on the RSM predicted too early separation as a result the subsequent vortex development is predicted poorly compared to the DDES based on SA-RC-QCR.

6.2.1. Discussion on RSM based DDES predictions

In the present work the RSM-DDES predicted earlier separation compared to RSM. The reason for earlier separation is most probably the blending function employed in the RSM-DDES computation. In the current investigation Menter's blending function F1 [16] is employed with which the RSM-DDES model switches from RANS to LES. Usually for RSM-DDES computations, Menter's blending function F2 [16] is employed. In the current investigation F1 is chosen to resolve the vortices which are located very close to the wall. Because of this, the RSM-DDES employed in the present work switches from RANS to LES within the attached boundary layer where the grid resolution is not fine enough and the flow too stable to quickly produce LES content. As a result lower total turbulent stresses within the boundary layer are predicted (so-called "modelled-stress depletion" [11]) which eventually lead to earlier flow separation in the RSM-DDES predictions than in RSM investigation.

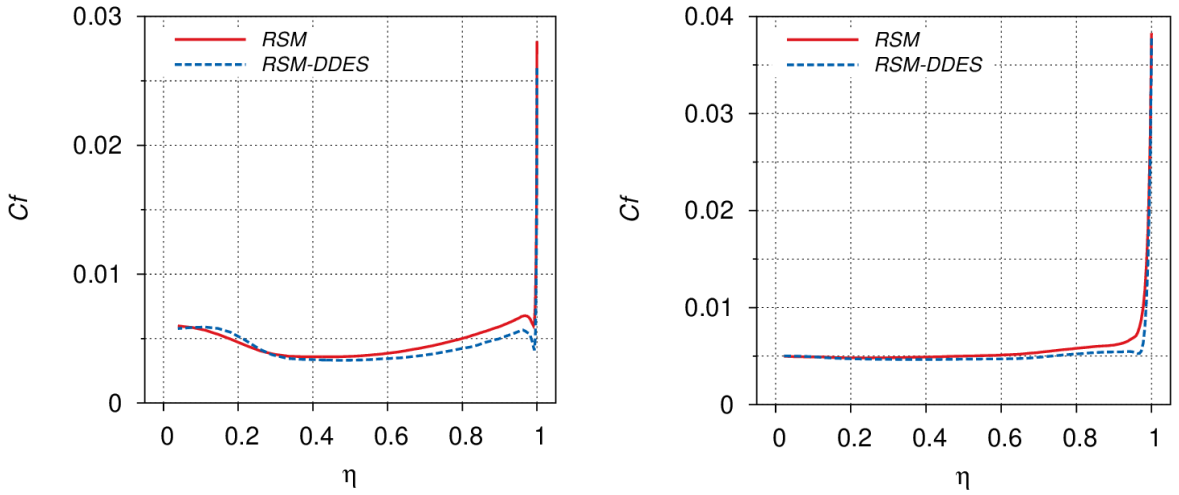

(a) Delta wing (b) Diamond wing

Figure 15: Cf along the wing span for delta and diamond wing

To demonstrate this, the cf along the wing span for the delta wing and diamond wing at x/c_r of 0.2 and 0.15, respectively, is shown in Figure 15. For both configurations, the cf is lower in RSM-

DDES than in RSM computations. The reason for this is the lower turbulence stresses in the boundary layer in RSM-DDES compared to RSM.
For future investigations, Menter's blending function F2 or the delay function f_d [14] used in SA-DDES are recommended, which are expected to improve the predictions of RSM-DDES for both configurations.

7. Summary

To assess the advantages of applying Reynolds stress model over scale-resolving simulation for separated vortex flows, investigations are carried out for the flow over a delta wing and a diamond wing. Both cases are characterized by separation from a smooth surface and subsequent vortex formation, the phenomena often observed on military configurations. Here, the main objective is to explore the performance of RSM compared to eddy-viscosity model (EVM) based hybrid RANS/LES methods (HRLM) and RSM based HRLM methods in the prediction of separated vortex flows. To this end, aforementioned configurations are investigated using the SSG/LRR-ln(ω) Reynolds stress model and the predictions are compared to the prediction delivered by EVM based HRLM and RSM based HRLM. In EVM based HRLM, the delayed detached eddy simulation based on SA and SA-RC-QCR are employed.

For the evaluation of hybrid RANS/LES, investigations are carried out with the SA-DDES and SA-RC-QCR-DDES for the delta and diamond wing. For both configurations, the SA-RC-QCR-DDES predicted separation too early and delivered weaker vortices and located more in board on the wing compared to the experiments. However, the SA-DDES predicted vortex separation close to experiments. In the case of delta wing, the SA-DDES predicted inner and outer primary vortices, but after a short downstream distance merging of the inner primary vortex with the outer primary vortex is observed. The trend delivered in the SA-DDES is different from the experiments. For the Diamond wing, both inner and outer primary vortices are predicted and the pressure associated with the outer primary vortex observed to be in good agreement with the experiments. Comparison of RSM and HRLM for the aforementioned configurations unveils that the RSM predicts the flow better than HRLM for delta wing while for Diamond wing, SA-DDES represents the flow better than RSM.

Finally, RSM-based DDES is employed to investigate the flow over the delta wing and diamond wing in order to explore the potential of the combination of both methods. For both configurations, RSM-DDES performed poorly by predicting too upstream vortex separation and weaker inner and outer primary vortices. It was found, however, that an unsuitable "shielding" function applied in these RSM-DDES computations may have caused modelled-stress depletion in the early boundary layer and, thus, the premature separation.

In spite of some degree of agreement between RSM predictions and experiments, still improvements in the predictions are required with regard to the strength and location of the inner primary and outer primary vortices.

Acknowledgements

The research presented in this report is funded by the Air Force office of Scientific Research (AFOSR), Award No. FA9550-18-1-7019. The funding is gratefully acknowledged.

References

[1] N. Frink, M. Tomac und A. and Rizzi, „Collaborative study of incipient separation on 53° swept diamond wing," *Aerospace Science and Technology,*Vol. 57, pp. 76-89, 2016.

[2] M. Ghoreyshi, K. Ryszka, R. Cummings und A. Lofthouse, „Vortical flow prediction of a diamond wing with rounded leading edges," *AerospaceScienceandTechnology,* vol. 57, pp. 103-117, 2016.

[3] S. Braun, U. A., B. Eisfeld und E. Stumpf, „Numerical Simulation of Vortex Roll-Up Processes Using the SSG/LRR-w," *New Results in Numerical and Experimental Fluid Mechanics X Notes on Numerical Fluid Mechanics and Multidisciplinary Design ,* Vol. 132, pp. 481-491, 2016.

[4] V. Togiti, V. Ciobaca, B. Eisfeld und T. Knopp, „Numerical simulation of steady blowing active flow control using a differential reynolds stress model," in *CEAS/KATnet II*, Bremen, Germany, 2009.

[5] D. Hummel und G. Redeker, „A new vortex flow experiment for computer code validation," in *RTO-AVT Symposium on Vortex Flow and High Angle of Attack*, Loen, Norway, 7–11 May, 2001.

[6] J. Luckring und D. Hummel, „What was learned from the new VFE-2 experiments," *Aerosp. Sci. Technol.,* Vol. 24, Nr. 1, p. 77–88, 2013.

[7] A. Hövelmann, M. Grawunder, A. Buzica und C. Breitsamter, „AVT-183 diamond wing flow field characteristics Part 2: Experimental analysis of leading-edge vortex formation and progression," *Aerospace Science and Technology,* Vol. 57, p. 31–42, 2016.

[8] T. G. Wetzel, R. L. Simpson und C. J. Chesnakas, „Measurement of three-dimensional crossflow separation," *AIAA Journal,* Vol. 36(4), pp. 557-568, 1998.

[9] M. L. Shur, M. K. Strelets, A. K. Travin und P. R. Spalart, „Turbulence Modeling in Rotating and Curved Channels: Assessing the Spalart-Shur Correction," *AIAA journal,* Vol. 38, No. 5, pp. 784-792, 2000.

[10] M. Mani, D. A. Babcock, C. M. Winkler und P. R. and Spalart, „Predictions of a Supersonic Turbulent Flow in a Square Duct," in *AIAA Paper 2013-0860*, 2013.

[11] P. Spalart, S. Deck, M. Shur, K. Squires, M. K. Strelets und A. Travin, „A New Version of Detached-Eddy Simulation, Resistant to Ambiguous Grid Densities," *Theoretical and Computational Fluid Dynamic 20, 1*81, 2006.

[12] B. Eisfeld, C. Rumsey und V. Togiti, „Verification and Validation of a Second-Moment-Closure Model," *AIAA Journal,* Vol. 54, No. 5, pp. 1524-1541, 2016.

[13] S. Braun, „Implementation of a ln(w) based SSG/LRR Reynolds Stress Model into the DLR-TAU Code," Institutsbericht, DLR-IB-AS-BS-2019-37, Report of the Institute of Aerodynamics and Flow Technology, Braunschweig, 2019.

[14] M. Gritskevich, A. Garbaruk, J. Schütze und F. Menter, „Development of DDES and IDDES Formulations for the k-ω Shear Stress Transport Model," *Flow Turbulence and Combustion* , Vol. 88, Nr. 3, p. 431–449, 2012.

[15] A. Probst, R. Radespiel und K. T., „Detached-Eddy Simulation of Aerodynamic Flow Using a Reynolds Stress Background Model and Algebraic RANS/LES Sensor," in *AIAA Paper No. 3206*, 2011.

[16] F. R. Menter, „Two-Equation Eddy-Viscosity Turbulence Models for Engineering Applications," *AIAA Journal,* Vol. 32, No. 8, pp. 1598-1605, 1994.

[17] D. Schwamborn, T. Gerhold und R. Heinrich, „The DLR TAU-Code: Recent Applications in Research and industry," in *Europen Conference on CFD, ECCOMAS CFD*, 2006.

[18] A. Probst, J. Lowe, S. Reuß, T. Knopp und R. Kessler, „Scale-Resolving Simulations with a Low-Dissipation Low-Dispersion Second-Order Scheme for Unstructured Flow Solvers," *AIAA Journal,* Bd. 54, Vol. 10, p. 2972–2987, 2016.

[19] V. Togiti, A. Krumbein und A. Probst, RANS investigations of vortex separated flows, Report of the Institute of Aerodynamics and Flow Technology, Braunschweig, DLR-IB-AS-BS-2022-62, 2022.

[20] P. R. Spalart und S. R. Allmaras, „ A One-Equation Turbulence Model for Aerodynamic Flows," in *Recherche Aerospatiale*, 1994.

DLR-IB-AS-BS-2022-63
Scale-resolving Simulation of Vortex Separated Flows

V. Togiti, A. Krumbein, A. Probst

Verteiler:

Institutsbibliothek AS	1 Exemplar
Verfasser/Co-Autoren je	1 Exemplar
Institutsleitung	1 Exemplar
Abteilungsleiter	1 Exemplar
Deutsche Bibliothek in Frankfurt/Main	2 Exemplare
Niedersächsische Landesbibliothek Hannover	1 Exemplar
Techn. Informationsbibliothek Hannover	1 Exemplar
Zentralbibliothek BS	1 Exemplar
Zentralarchiv GÖ	1 Exemplar
Reserve	1 Exemplar